1q gain and CDT2 overexpression underlie an aggressive and highly proliferative form of Ewing sarcoma

Mackintosh, C.; Ordonez, J.L.; Garcia-Dominguez, D.J.; Sevillano, V.; Llombart-Bosch, A.; Szuhai, K.; ... ; Alava, E. de

Oncogene (2012) 31, 1287–1298

www.nature.com/onc

ORIGINAL ARTICLE

1q gain and *CDT2* overexpression underlie an aggressive and highly proliferative form of Ewing sarcoma

C Mackintosh[1], JL Ordóñez[1], DJ García-Domínguez[1], V Sevillano[1], A Llombart-Bosch[2], K Szuhai[3], K Scotlandi[4], M Alberghini[5], R Sciot[6], F Sinnaeve[7], PCW Hogendoorn[8], P Picci[4], S Knuutila[9], U Dirksen[10], M Debiec-Rychter[11], K-L Schaefer[12] and E de Álava[1,13]

[1]*Molecular Pathology Program, Centro de Investigación del Cáncer-IBMCC (USAL-CSIC), Campus Miguel de Unamuno S/N, Salamanca, Spain;* [2]*Department of Pathology, University of Valencia, Valencia, Spain;* [3]*Department of Molecular Cell Biology, Leiden University Medical Center, Leiden, The Netherlands;* [4]*Laboratory of Oncologic Research, Istituti Ortopedici Rizzoli, Bologna, Italy;* [5]*Department of Pathology, Istituti Ortopedici Rizzoli, Bologna, Italy;* [6]*Department of Pathology, Catholic University of Leuven, Leuven, Belgium;* [7]*Department of Orthopedic Surgery, Catholic University of Leuven, Leuven, Belgium;* [8]*Department of Pathology, Leiden University Medical Center, Leiden, The Netherlands;* [9]*Department of Pathology; University of Helsinki and Helsinki University Central Hospital, Helsinki, Finland;* [10]*University Children's Hospital Muenster, Department of Pediatric Hematology and Oncology, Muenster, Germany;* [11]*Center for Human Genetics; Catholic University of Leuven, Leuven, Belgium;* [12]*Institute of Pathology; Heinrich-Heine-University Duesseldorf, Duesseldorf, Germany and* [13]*Department of Pathology, University Hospital of Salamanca, Salamanca, Spain*

Despite extensive characterization of the role of the EWS-ETS fusions, little is known about secondary genetic alterations and their clinical contribution to Ewing sarcoma (ES). It has been demonstrated that the molecular structure of EWS-ETS lacks prognostic value. Moreover, *CDKN2A* deletion and *TP53* mutation, despite carrying a poor prognosis, are infrequent. In this scenario identifying secondary genetic alterations with a significant prevalence could contribute to understand the molecular mechanisms underlying the most aggressive forms of ES. We screened a 67 ES tumor set for copy number alterations by array comparative genomic hybridization. 1q gain (1qG), detected in 31% of tumor samples, was found markedly associated with relapse and poor overall and disease-free survival and demonstrated a prognostic value independent of classical clinical parameters. Reanalysis of an expression dataset belonging to an independent tumor set ($n = 37$) not only validated this finding but also led us to identify a transcriptomic profile of severe cell cycle deregulation in 1qG ES tumors. Consistently, a higher proliferation rate was detected in this tumor subset by *Ki-67* immunohistochemistry. *CDT2*, a 1q-located candidate gene encoding a protein involved in ubiquitin ligase activity and significantly overexpressed in 1qG ES tumors, was validated *in vitro* and *in vivo* proving its major contribution to this molecular and clinical phenotype. This integrative genomic study of 105 ES tumors in overall renders the potential value of 1qG and *CDT2* overexpression as prognostic biomarkers and also affords a rationale for the application of already available new therapeutic compounds selectively targeting the protein-ubiquitin machinery.
Oncogene (2012) **31,** 1287–1298; doi:10.1038/onc.2011.317; published online 8 August 2011

Keywords: Ewing sarcoma; 1q Gain; *CDT2*; clinical outcome; microarrays

Introduction

Ewing sarcoma (ES) is an aggressive neoplasm of the bone and soft tissues mainly of children and young adults. Despite continuous therapeutic improvements, 5-year survival rates are below 20% in patients with advanced disease (Haeusler *et al*., 2010). At molecular level, the main feature of ES is the presence of specific balanced chromosomal translocations, which give rise to oncogenic chimeric proteins (EWS-ETS), the most common being EWS-FLI1 as a consequence of the t(11;22)(q24;q12) translocation (Aurias *et al*., 1984; Turc-Carel *et al*., 1984; Whang-Peng *et al*., 1984; Delattre *et al*., 1992).

Although there is an extensive knowledge about EWS-ETS chimeric proteins (considered the initiating molecular event in the pathogenesis of the disease) (Ordoñez *et al*., 2009), few studies have evaluated the role of secondary genetic alterations in the oncogenesis and/or progression of ES. *TP53* mutations and *CDKN2A* deletions are known to confer poor prognosis but are infrequent in this tumor entity (around 13% percent of cases) (Huang *et al*., 2005).

Likewise, while major efforts in the copy number alteration (CNA) profiling of ES have succeeded in assessing the frequency of recurrent genomic alterations (Knuutila *et al*., 1998; Kullendorff *et al*., 1999; Tarkkanen *et al*., 1999; Brisset *et al*., 2001; Ozaki

Correspondence: Dr C Mackintosh or Dr E de Álava, Molecular Pathology Program, Centro de Investigación del Cáncer-IBMCC (USAL-CSIC), Campus Miguel de Unamuno S/N, Salamanca 37007, Spain.
E-mail: cmackintosh@usal.es or edealava@usal.es
Received 8 March 2011; revised 23 May 2011; accepted 21 June 2011; published online 8 August 2011

et al., 2001; Hattinger *et al*., 2002; Roberts *et al*., 2008), few have integrated genomic and transcriptomic profiles and gained in-depth information about their correlation with clinical parameters (Ferreira *et al*., 2008; Savola *et al*., 2009). Moreover, there is a substantial disagreement about which particular CNAs are clinically relevant in ES (Kullendorff *et al*., 1999; Tarkkanen *et al*., 1999; Brisset *et al*., 2001; Ozaki *et al*., 2001; Hattinger *et al*., 2002), probably because of the small size of the sample series analyzed (Knuutila *et al*., 1998; Kullendorff *et al*., 1999; Tarkkanen *et al*., 1999; Ferreira *et al*., 2008; Savola *et al*., 2009) and/or the use of techniques with low resolution/sensitivity (Knuutila *et al*., 1998; Kullendorff *et al*., 1999; Tarkkanen *et al*., 1999; Brisset *et al*., 2001; Ozaki *et al*., 2001; Hattinger *et al*., 2002), as most previous reports relied on karyotyping and/or metaphase CGH.

Given that the primary event (EWS-ETS) is now known to lack prognosis value (Le Deley *et al*., 2010; van Doorninck *et al*., 2010), secondary genetic alterations have emerged as likely candidates to account for the most aggressive forms of ES, and could eventually become molecular targets of specific therapies.

Here we report the marked impact of CNAs on ES clinical outcome, together with the identification of 1q gain (1qG) as the second most prevalent and the most clinically relevant CNA in this neoplasm. The integration of this genomic information layer with ES transcriptomic profiles has unveiled a severe deregulation of the cell cycle controls present in 1qG ES. *In vitro* and *in vivo* validations of *CDT2* support a major role for this 1q gene in this molecular and clinical phenotype.

Results

CNA profiling of ES tumors and cell lines provided a collection of minimal regions of CNA, useful for the identification of candidate genes

A total of 67 ES tumors from untreated patients (tumor set 1) and 16 ES cell lines were screened for CNAs by array CGH (aCGH). aCGH chips were scanned and sequentially processed with GenePix Software (data acquisition, flagging of bad-quality spots and normalization) and with the BioConductor packages CGHcall (van de Wiel *et al*., 2007) (segmentation and calling of the raw log2ratios), CGHregions (van de Wiel and Wieringen, 2007) (complexity reduction and partition into major genomic regions of CNA) and CGHtest (van de Wiel *et al*., 2005) (correlation with clinical parameters).

CNA frequency and distribution are summarized in Figure 1a and Supplementary Figures S1A–C and the amount of genome affected by CNA is depicted in Figure 1b. The profile of recurrent alterations obtained is similar to that described in previous reports: most frequent gains comprised the entire chromosome (chr) 8, and the chr arms 1q and 12p, while most frequent losses were located in 3p, 9p, 16q and 17p. Notwithstanding, the overall frequencies detected in ES tumors are noticeably higher than those previously reported (Supplementary Figure S1D), indicating a higher sensitivity of the technology and/or the analysis used in this study.

Due to the complexity of the RM82 CNA profile observed by aCGH, combined binary ratio labeling fluorescence *in situ* hybridizations (COBRA-FISH) of 18 metaphases of this cell line were evaluated in order to shed light into its chromosomal rearrangements and exact chr copy numbers. This chr painting approach validated the aCGH data, as both techniques demonstrated an outstanding agreement of their results (Supplementary Figures S2A and B).

Remarkably, although *CDKN2A* deletion (9p21.3) was one of the most frequent CNAs in cell lines (62.5%), it was detected only in eight tumors (12%), in five of them as a single-BAC (bacterial artificial chromosome) microdeletion (Figure 1c). The same can be said of the hemizygous deletions encompassing the *TP53* locus (17p13.1), which were frequently found in cell lines (37.5%) but were uncommon in the tumor samples (13.4%). Both CNA frequencies are in line with those previously reported for these loci (Huang *et al*., 2005).

Smallest regions of overlap (SRO) under 10 Mb in size and with a frequency above 35% were defined using the CNA profiles of both ES tumor samples and cell lines. SRO are the minimum region shared by all the samples carrying a particular CNA and are useful for the definition of short lists of genes with a potential oncogenic/tumor suppressor role (usually referred to as candidate genes). A summary of the SRO and the major candidate gene contained in each of them can be found in Supplementary Table S1. Worthy of note, the SRO in 8q24.13–q24.21 (6.8 Mb in size) was found amplified in three cell lines, and gained in all but one of them (93.75%), and it was also the most frequent CNA in the tumor samples (39%). Among others, this SRO spans the locus of the *MYC* gene.

Affymetrix 500K single-nucleotide polymorphism (SNP) microarray was used to accurately delimit small microdeletions like the one detected in 16q23.2. The SNP microarray revealed a deletion of 1.04 Mb in size, with breakpoint regions within a range of 4982–12603 bp (see Supplementary Figure S2C). We expect this SRO to be useful for the candidate gene mining of this region, the most frequent genomic loss in ES. However, restoring the expression levels of two candidate genes in 16q23.1 did not have any effect on the ES cell lines tested (C Mackintosh *et al*., unpublished data).

CNAs are secondary genetic alterations with a dramatic impact on ES patient survival

The parameter percentage of genome altered (PGA), which reliably reflects the total amount of genome affected by CNAs per sample, was divided in four ranges (see Supplementary Material and methods for details) and used to evaluate the impact of these secondary genetic alterations on ES patient survival. As a result, PGA increasing levels were found related to a gradual decrease in survival, by Kaplan–Meier log-rank tests (Figure 2a). Remarkably, those patients

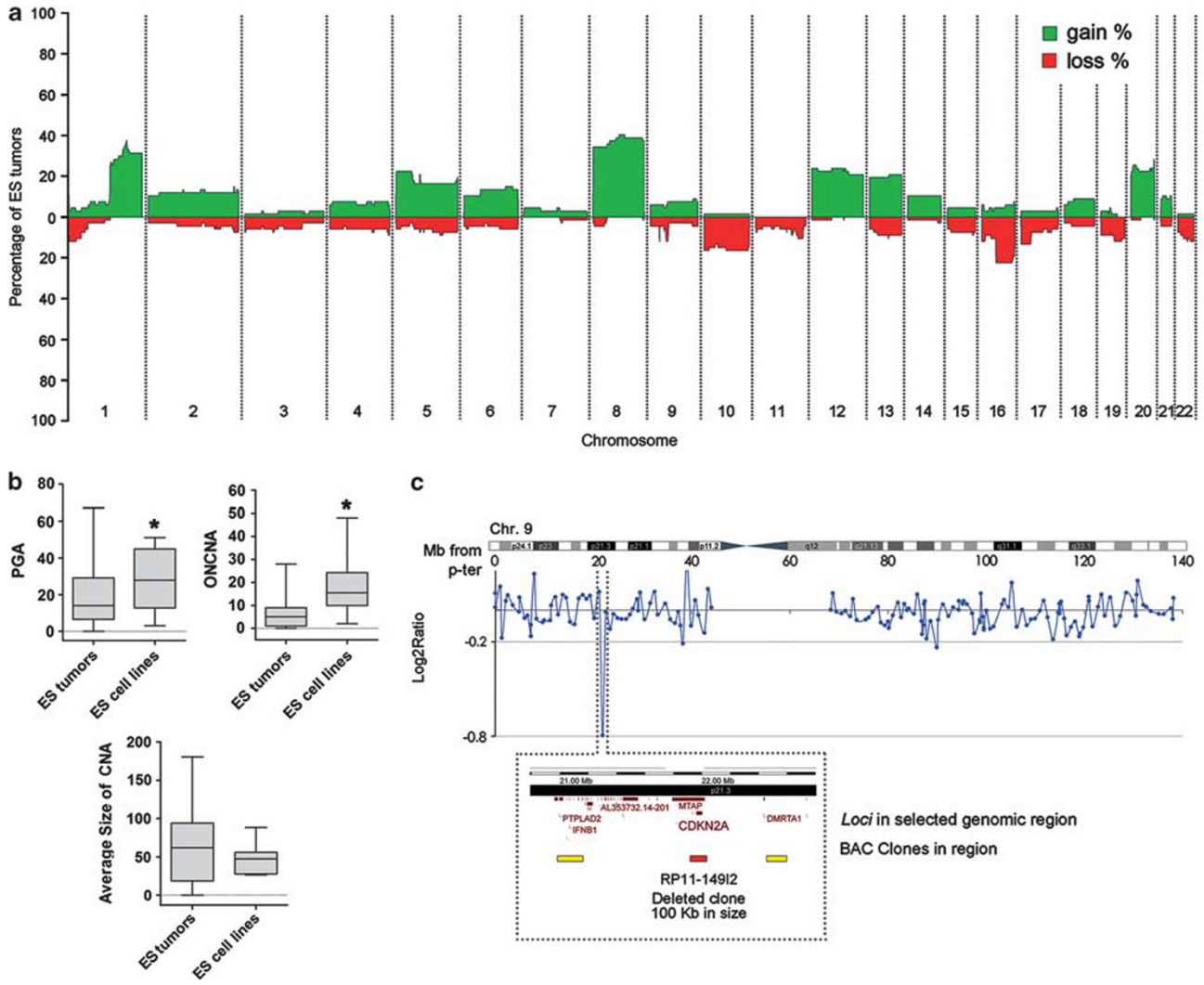

Figure 1 Summary of the CNAs detected in ES tumors and cell lines. (**a**) Frequency of the CNAs detected in ES tumor samples sorted by genomic position (from p-ter to q-ter) and by chr. Gain of genomic material is depicted in green while loss is depicted in red. (**b**) Boxplots illustrating the parameters PGA, overall number of CNAs (ONCNA) and average size of CNA of both ES tumors and cell lines. An expected higher presence of CNAs (*) in ES cell lines was observed (*t*-test *P*-values < 0.05), although the average size of CNA was similar in both sort of samples. (**c**) Illustration of the STAET2.1 ES cell line *CDKN2A* microdeletion, demonstrating the ability of the aCGH platform used in detecting this small CNA. Mb, megabases.

whose tumors lacked CNAs (PGA $<0.1\%$) had a very good survival (over 85% at 5 years). These observations suggest that it is not an arbitrary CNA threshold of 3 or 5, as reported by others (Ozaki *et al*., 2001; Ferreira *et al*., 2008; Savola *et al*., 2009), but the presence and amount of CNAs that are determining the worse clinical outcome of those ES patients with tumors affected by chromosomal instability.

1qG has a profound impact on the clinical outcome of ES patients

Once confirmed the relevance of the CNAs as a whole in ES, the bioinformatics package CGHtest (van de Wiel *et al*., 2005) was applied in order to unravel the clinical contribution of particular CNAs. CGHtest includes the bioinformatics scripts CGHpermutation and CGHlogRank. CGHpermutation assesses the differential enrichment of particular CNAs in the clinical circumstances compared (for instance, metastatic primary tumors versus non-metastatic primary tumors), enabling the detection of any existing association between CNAs and clinical parameters. CGHlogRank detects any CNA related to a difference in patient survival, through Kaplan–Meier log-rank tests. Both scripts implement multiple testing correction, represented by the false discovery rate (FDR) *q*-values included in Supplementary Table S2.

As a result of these tests (described in Supplementary Table S2, test type: CGHpermutations) we were able to identify 1qG (detected in 31% of tumors) as the CNA with the highest clinical impact, because:

(1) It was the only CNA significantly enriched in tumors from ES patients who suffered progression of the disease (either local relapse or distant metastasis; Supplementary Table S2, test #1). Indeed, more than half of the primary tumors that

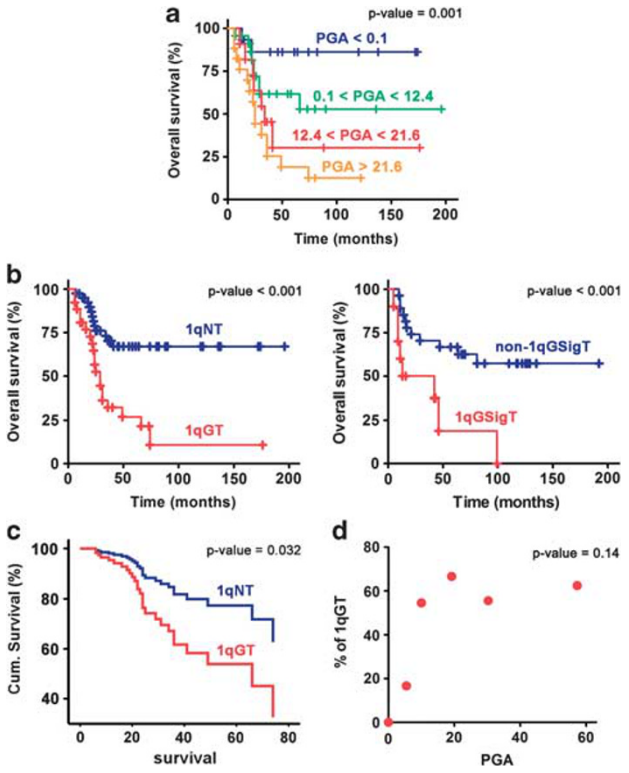

Figure 2 CNAs are secondary genetic events with a dramatic impact on the clinical outcome of ES patients. (**a**) Kaplan–Meier log-rank test showing the association of the PGA parameter, divided in four ranges, with a gradual poorer overall survival of ES patients. (**b**) Kaplan–Meier log-rank test of 1qG (left panel) and 1qGSigT (right panel) demonstrating the association of the 1qG CNA with a poorer overall survival of ES patients. (**c**) Multivariate Cox regression model of 1q CNA status. (**d**) Dotplot of PGA (median value of six equally distributed population ranges) and 1qGT (percentage of 1qGT in each PGA range), proving the absence of correlation between both parameters. *P*-values of each test are shown in the corresponding figure panel.

developed clinical relapse (55%) carried gains in this chr arm, whereas only 11.5% of non-relapsing tumors.

(2) It was the CNA associated with the most significant difference in survival, with both a poorer overall survival and disease free survival, (Figure 2b, left panel; Supplementary Table S2, test type: CGHlogRank). No other CNA was found related to differences in both overall survival and disease free survival. Moreover, Cox regression analysis confirmed the prognostic value of the 1q CNA status, independent of classical prognostic parameters (metastasis and tumor size; *P*-value = 0.032; Figure 2c; Supplementary Table S3).

The impact of 1qG on survival was confirmed in an independent ES tumor set (tumor set 2), using a 1qG local expression signature (the 1qGSig, see below), as depicted in Figure 2b, right panel.

1qG clinical impact is not a reflect of the PGA value or of other CNAs

Given that PGA demonstrated a dramatic impact on ES patient survival, the observed 1qG association with a worse clinical outcome could be reflecting a hidden correlation between both parameters. However, a Pearson correlation test comparing the median PGA value of the ranges shown in Figure 2a and the percentage of 1qG ES tumors (1qGT) in each range ruled out this possibility (*P*-value = 0.22). Further partitioning of the data according to six ranges delimited by equally distributed PGA percentiles did not reach statistical significance either (*P*-value = 0.14), as shown in Figure 2d.

Regarding the association of 1qG with other genomic alterations, several CNAs were found to specifically appear in 1qGT: gains of the entire chr 12 and chr 20, and loss of 16q (Supplementary Table S2, test #10). This does not mean that 1qG is always accompanied by these CNAs (which indeed are less frequent), but that they tend to occur preferentially in 1qGT. The association between 1qG and 16q loss (10 out of 25 1qGT carried the 16q loss) was expected and represents a validation of the analysis, as unbalanced translocations between both chr arms are known to account for a portion of the 1qG events (Hattinger *et al*., 1996). Anyway, no differences in overall survival were found between patients with the 1qG alone and patients with both 1qG and any of its associated CNAs (neither single, nor multiple associations; data not shown), discarding a clinical contribution of said CNAs by themselves.

Remarkably, no statistical association was found between 1qG and losses of 9p21.3 or 17p13.1, the genomic regions that harbor *CDKN2A* and *TP53* loci (Supplementary Table S2, test #10).

1qG is linked to an expression pattern of cell cycle deregulation and to an increased cell proliferation rate

In order to evaluate the effect of 1qG on the main cellular processes and functions we re-analyzed a publicly available dataset from a previous expression microarray study belonging to an independent ES tumor set (tumor set 2, $n = 38$) (Scotlandi *et al*., 2009). Moreover, 14 out of the 38 samples from this tumor set have been also CNA profiled, and the genomic data produced is publicly available as well (Savola *et al*., 2009). Using the expression dataset from this 14-tumor subset with known CNA status we defined a local expression signature, the 1qG local signature (1qGSig), by first performing a differential expression analysis comparing 1qGT ($n = 6$) versus 1q normal ES tumors (1qNT; $n = 8$) and then selecting those genes located in 1q with the highest *d*-values and fold-change values (cutoffs settled: *d*-value > 4.9, the 90th percentile; fold change, R-fold > 1.5; 74 1q genes satisfied both requirements). The gene composition of the 1qGSig is included in Supplementary File 1, Spreadsheet #1.

The entire 38-tumor set was subjected then to hierarchical clustering using their expression values for the 1qGSig genes. As a result, those samples known to have the 1qG were contained in cluster 1 (Figure 3a), clearly segregated from the 1qNT (included in cluster 2 and 3). Hence, we assumed that the 1qGSig is able to reflect the underlying 1q CNA status and that those

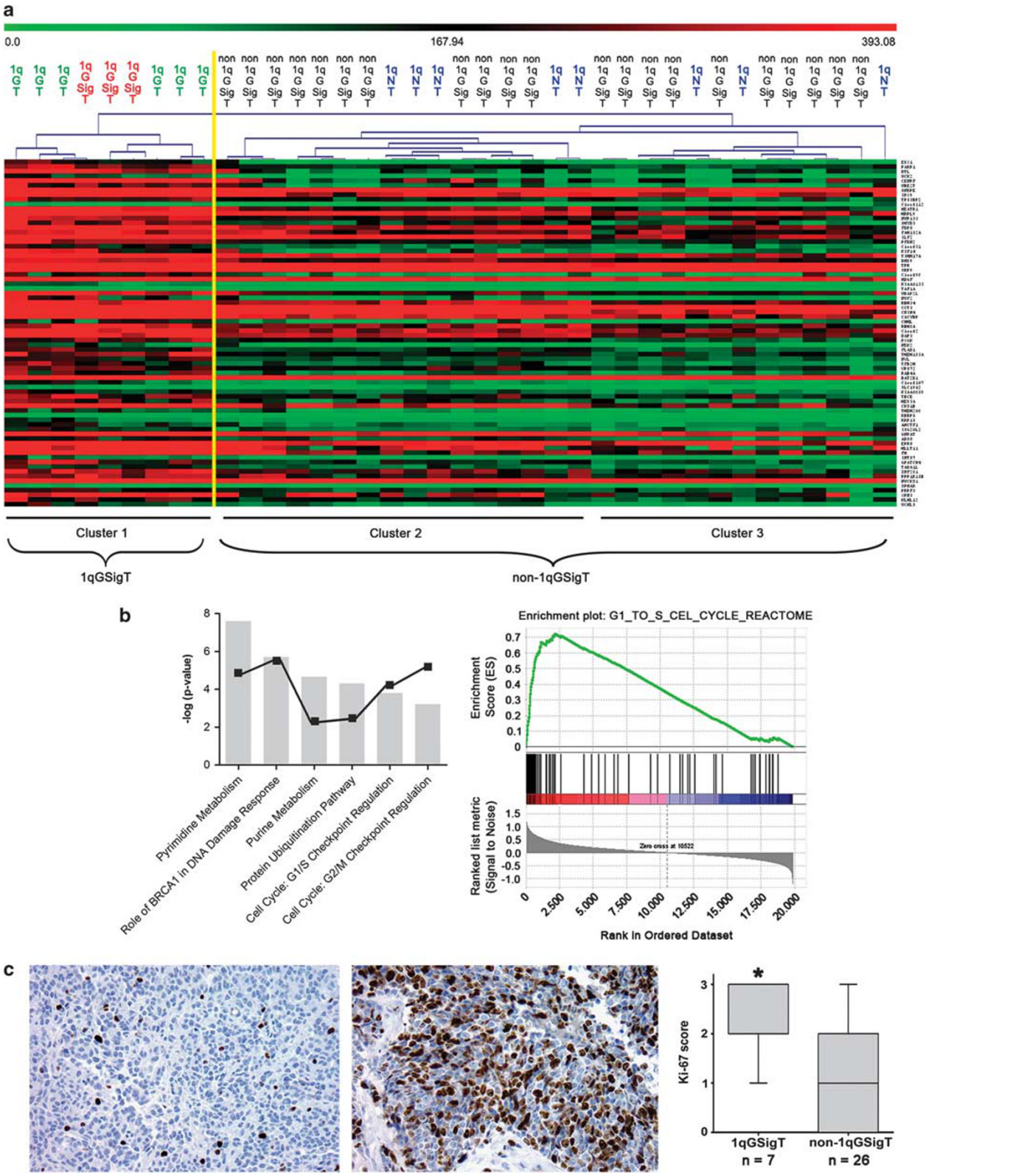

Figure 3 1qG is linked to an expression pattern of cell cycle deregulation and higher proliferation rates in ES. (**a**) Hierarchical clustering showing 1qGSig ability to segregate ES tumors according to their underlying 1q CNA status, identifying additional tumors presumably bearing the 1qG (cluster 1, 1qGSigT, in red). 1qGT, in green: tumors known to bear the 1qG; 1qNT, in blue: tumors known not to bear the 1qG. (**b**) IPA (left panel) and GSEA (right panel, representative enrichment plot) results predicted the existence of a severe cell cycle deregulation in 1qGSigT. (**c**) *Ki-67* IHC validated the IPA and GSEA analyses: 1qGSigT showed higher *Ki-67* scores (left panel: *Ki-67* negative non-1qGSigT; central panel: *Ki-67* positive 1qGSigT; right panel: boxplot summarizing the *Ki-67* IHC scores). *Kendall–Tau and Mann–Whitney *U*, *P*-values <0.05.

samples in cluster 1 without known copy-number status bear the 1qG CNA as well. We designated the ES tumors included in cluster 1 as 1qGSig tumors (1qGSigT). Similarly, we will refer to those ES tumors in clusters 2 and 3 as non-1qGSig tumors (non-1qGSigT).

Next, gene set enrichment analysis (Subramanian *et al*., 2005) (GSEA; 1qGSigT versus non-1qGSigT, using their complete expression data) detected an increased expression of MYC and E2F1 upregulated targets, G1 to S transition activators, genes that promote DNA replication, and genes known to be downregulated by ectopic *p21* overexpression (therefore predicting a loss of *p21* function), among others (Table 1). These results obtained very low FDR *q*-values and high normalized enrichment scores, revealing the existence of a severe cell cycle deregulation in 1qGSigT, probably caused by the loss of multiple cell cycle controls. Figure 3b, right panel, displays the enrichment plot of the gene set 'G1 to S transition reactome', which obtained the highest normalized enrichment score. In addition, the results from the Molecular Signatures Database Collection 1 confirmed the overrepresentation of 1q genes and discarded any significant contribution of the 1qG-associated CNAs to the expression pattern of 1qGSigT (Table 1). An explanation of the GSEA basics is included in Supplementary Material and methods. Complete lists of the GSEA results can be found in Supplementary File 1, Spreadsheets #2 to #5. Gene set compositions can be obtained at http://www.broadinstitute.org/gsea/msigdb/genesets.jsp.

Ingenuity Pathway Analysis (IPA) was applied to validate GSEA results. Cell cycle and cancer were found to be the most significant functions overrepresented in 1qGSigT. In addition, IPA found DNA metabolism (of both pyrimidine and purine), G1/S checkpoint regulation, G2/M checkpoint regulation and protein ubiquitination pathway to be among the most significantly altered canonical pathways (Figure 3b, left panel).

We considered this redundancy between IPA and GSEA to be highly meaningful and assumed that, according to both bioinformatics predictions, 1qGSigT should have higher proliferation rates. In order to validate this assumption, a tissue microarray composed of 33 samples belonging to tumor set 2 was obtained and used for the immunohistochemical analysis (IHC) of *Ki-67*, a well-established marker of proliferation. The IHC was scored with four values, according to the observed percentage of immunostained cells. As a result, 1qGSigT were confirmed to have significantly higher *Ki-67*-proliferation rates (Figure 3c, Kendall–Tau = 0.008, Mann–Whitney $U = 0.02$). Examples of a negative and a positive tumor (scored 3) for *Ki-67* IHC can be found in Figure 3c.

Table 1 Most representative gene sets found enriched in 1qGSigT by GSEA

	Size	*NES*	*NOM P-value*	*FDR q-value*
C2 MsigDB				
G1 to S cell cycle reactome	68	2.193	0.000	0.001
Pyrimidine metabolism	57	1.989	0.000	0.005
P21 any dn	34	1.967	0.000	0.006
Ren e2f1 targets	38	1.945	0.000	0.006
Schumacher myc up	49	1.938	0.000	0.006
C3 MsigDB				
V$E2F Q4 01	185	2.128	0.000	0.002
V$E2F1DP1 01	185	2.009	0.002	0.002
V$E2F1 Q6 01	192	1.998	0.002	0.002
V$MYC Q2	152	1.799	0.000	0.010
V$MYCMAX 01	215	1.763	0.000	0.015
C5 MsigDB				
Cell cycle go 0007049	294	2.114	0.000	0.015
Regulation of cell cycle	170	2.108	0.000	0.006
Mitotic cell cycle	140	2.098	0.000	0.004
DNA replication	93	2.095	0.000	0.004
G1 to S transition of mitotic cell cycle	27	1.971	0.002	0.006
Regulation of cyclin-dependent protein kinase activity	42	1.942	0.000	0.008
C1 MSigDB				
CHR1Q44	42	2.333	0.000	0.000
CHR1Q42	102	2.187	0.000	0.006
CHR1Q25	73	2.022	0.002	0.034
CHR1Q22	67	1.960	0.002	0.053
CHR1Q21	212	1.915	0.002	0.057
CHR1Q41	36	1.779	0.005	0.105
CHR1Q24	48	1.720	0.014	0.147
CHR1Q32	143	1.666	0.014	0.210
CHR1Q23	78	1.630	0.014	0.235

Abbreviations: FDR, false discovery rate; GSEA, gene set enrichment analysis; NES, normalized enrichment score; NOM, nominal *P*-value. Selection of the most representative gene sets found enriched in 1qGSigT, ordered by MSigDB gene set collection (C1–C3 and C5, see Supplementary Material and methods). Size = number of genes included in the gene set. A complete list of enriched gene sets can be found in Supplementary File 1, Spreadsheets #2 to #5.

CDT2 *is the gene most significantly overexpressed in 1qGSigT and its function fits with the bioinformatics findings*

In order to confirm empirically the link between the 1qG and the cell cycle deregulation, we established the following requirements for candidate gene selection:

(1) Location in 1q.
(2) Significantly overexpressed in 1qGSigT: genes at the top of the *d*-value ranked list from the differential expression analysis (1qGSigT versus non-1qGSigT). The *d*-value parameter from the significance analysis of microarrays (SAM) test combines the difference in expression between the groups compared and intra-group dispersion corrections. Therefore, it is the most reliable differential expression value.
(3) Genes with fold-changes above the value expected due to the underlying change in 1q genomic dosage (R-fold > 3; expected 1.5).
(4) Genes with functions directly involved in cell cycle control.
(5) Genes involved in as many as possible of the deregulated canonical pathways found by the IPA.

Only one gene satisfied all these requirements: *CDT2*. Briefly, *CDT2* (*DTL, L2DTL* and *RAMP* are other gene synonyms), a gene located in 1q32.3 at 212.2 Mb from p-ter, was the most significantly overexpressed gene (it ranked first in the 1qGSigT differential profile, *d*-value = 11.9) and it was also the 1q gene with the highest fold-change (R-fold = 4.78). The 1qGSigT differential expression profile, composed of 319 genes, is included in Supplementary File 1, Spreadsheet #6 (SAM list, FDR *q*-value <0.001).

Regarding *CDT2* tissue expression pattern and function, its levels are crucial during mouse early embryonic development, whereas in adult humans and mice its expression is restricted to actively dividing tissues (Liu *et al*., 2007; Supplementary Figure S3). In addition, it takes part in an ubiquitin ligase complex ($CUL4/DDB1^{CDT2}$), specifically involved in the selection of the substrates that are subsequently ubiquitinated by the complex (Jin *et al*., 2006; Higa *et al*., 2006b). $CUL4/DDB1^{CDT2}$ complex substrates are well-known G1 to S transition and DNA synthesis regulators (*p53*, *p21*, *p27* and *CDT1*, among others) (Banks *et al*., 2006; Ralph *et al*., 2006; Sansam *et al*., 2006; Higa *et al*., 2006a, c; Abbas *et al*., 2008; Kim *et al*., 2008; Nishitani *et al*., 2008). Thus, *CDT2* is a multiple cell cycle regulator and its function matches most of the GSEA and IPA predictions, connecting cell cycle control, DNA replication and protein ubiquitination pathways.

CDT2 probeset levels from tumor set 2 expression dataset were used to validate the association of *CDT2* overexpression (defined as an expression higher than the 75th percentile of *CDT2* probeset levels) with a poorer survival of ES patients (Supplementary Figures S4A and B).

RNA from 14 ES tumors (including seven 1qGSigT) belonging to tumor set 2 was obtained. Real-time reverse transcription–quantitative PCR (RT–qPCR) confirmed the difference in *CDT2* mRNA levels between 1qGSigT and non-1qGSigT predicted by the expression microarray (Supplementary Figure S4C). The fold change obtained (ratio of medians = 3.9; ratio of means = 4.79) was similar to that found by the microarray (R-fold = 4.78). Similarly, and despite the lack of protein extracts from tumor samples, higher *CDT2* protein levels were observed in 1qG ES cell lines by western-blot (Supplementary Figure S4D).

CDT2 *tightly regulates the G1 to S transition and proliferation of 1qG ES cell lines*

Five pLKO.1-shRNA (small hairpin RNA) constructions, each one targeting a different region of the *CDT2* transcript (Supplementary Table S4), were tested in RM82, an ES cell line with 1qG and high *CDT2* protein levels (Supplementary Figure S4D). A low multiplicity of infection (moi) was used (moi = 3). All the constructions tested decreased *CDT2* protein levels with different efficiencies (Figure 4a, left panel). Three of the constructions were tested further and were confirmed to induce G0/G1-cell cycle arrest (Figure 4a, right panel) and apoptosis (Figure 4a, left panel, anti-cleaved caspase-3 blot). Two of these shRNA constructions (sh280 and sh2495) were selected for functional validations due to their *CDT2* knockdown and cell cycle arresting efficiencies, and because together they cover a wider range of *CDT2* isoforms.

Next, *CDT2* knockdown was performed in two cell lines: RM82 and TC32 (that also carries the 1qG and has high *CDT2* levels too; Supplementary Figure S4D). We opted for a gradual silencing approach, achieved by progressively diluting the viral supernatant used for cell transduction. With this approach, *CDT2* endogenous overexpression was reduced according to several silencing levels (Figure 4c), allowing functional studies to be carried out (as *CDT2* complete knockdown, obtained only at a very high moi, arrests 90% of cell population in G0/G1 and induces massive apoptosis; Supplementary Figure S5A).

A pLKO.1-turboGFP construction was transduced in parallel to calculate the moi, confirming the complete population transduction achieved in the entire range of silencing levels (Figure 4b). Likewise, a pLKO.1-non-targeting control (NTC) construction was used in every assay to estimate the off-target effects.

Transduced cells were subjected to cell cycle, apoptosis and proliferation assays. The results obtained revealed that *CDT2* regulates the S-phase entry of 1qG ES cell lines, insomuch that the silencing level and the corresponding percentage of cell population in S-phase fitted in a linear regression (Figure 4d, left panel). Induction of apoptosis was also gradual (Figure 4d, right panel), although notably higher in TC32 than in RM82, which could be explained by the absence of *p21* induction in the latter (see below and Figure 6a). Furthermore, a gradual decrease in cell proliferation was also detected (Supplementary Figure S5B).

We discarded the insertion of the lentiviral constructions into the host genome as the cause of the changes observed after reproducing the same results by siRNA knockdown. The effect of the siRNA on *CDT2* protein levels was confirmed in a 3-day time lapse in which assays were conducted (Figure 4e, left panel). This approach, which does not involve insertional events, also resulted in G0/G1 cell cycle arrest and apoptosis induction (Figure 4e, central and right panels).

Similarly, a pBABE-*CDT2* construction was transduced in STAET2.1, a 1q normal ES cell line with low *CDT2* levels (Supplementary Figure S4D). Functional tests were carried out with a multiclonal population transduced with a moi = 1, intended to avoid artefactual levels of expression. In consequence, a three-fold increase in *CDT2* protein levels was achieved (Figure 4f, left panel). This mild overexpression was enough to induce a detectable increase in the proliferation rate, along with a decrease in the G2/M cell population (Figure 4f, central and right panels), consistent with the known requirement of *CDT2* for the G2/M checkpoint onset (Sansam *et al*., 2006). This finding highlights *CDT2* pleiotropic effects on cell cycle.

Finally, RM82 and TC32 cell lines were injected subcutaneously in mice after gradual silencing of *CDT2* (Figure 5a). *In vivo* results confirmed the effects

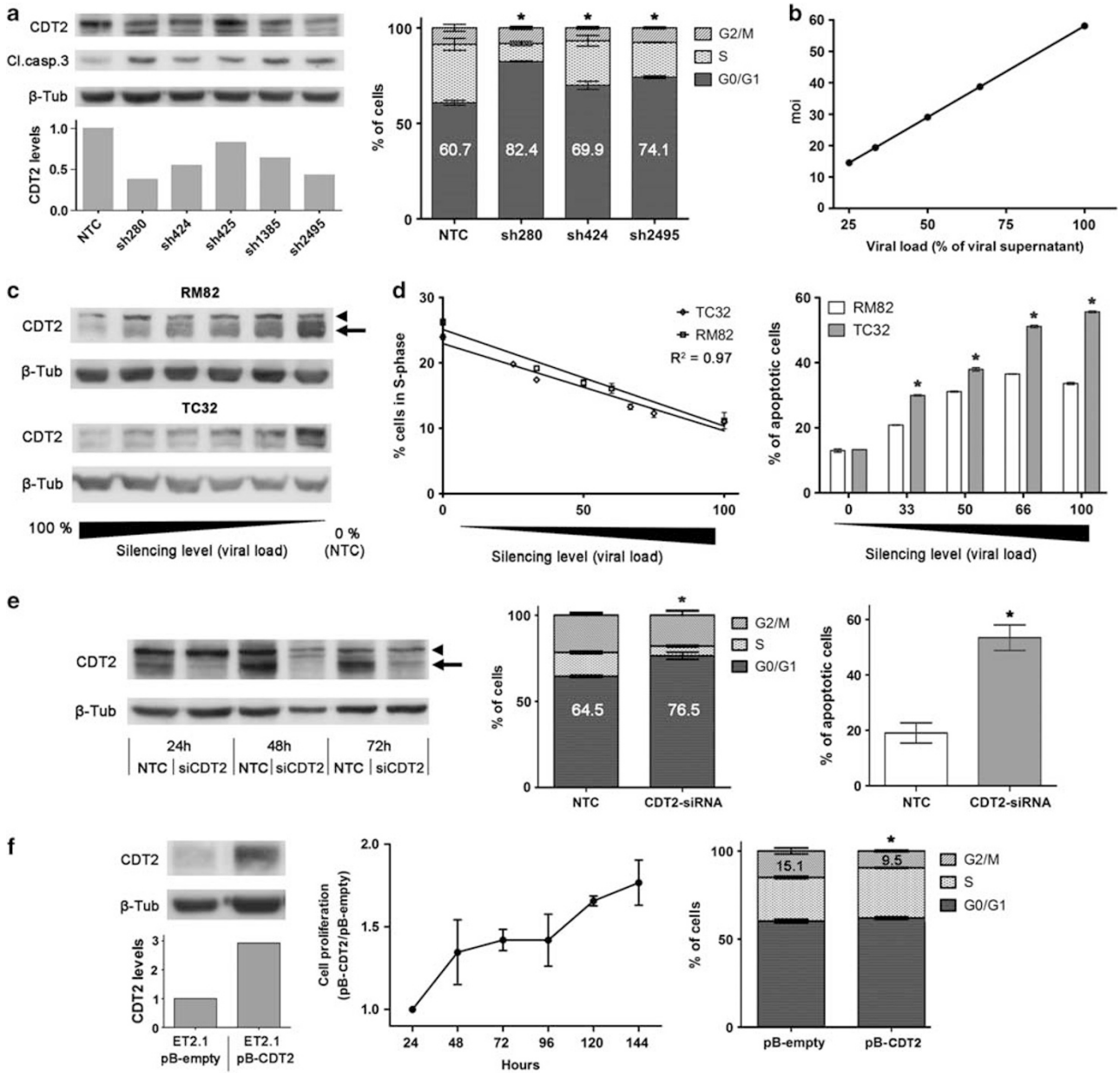

Figure 4 *CDT2* tightly regulates the entry in S-phase of 1qG ES cell lines, while its ectopic overexpression in a 1q normal ES cell line induced an increase in proliferation. (**a**) Several of the 5 shRNA constructions tested were able to efficiently decrease *CDT2* levels (left panel; barplot: levels of *CDT2* normalized to β-tubulin levels, blot quantification) and to induce G0/G1-cell cycle arrest (right panel) and apoptosis (left panel: cleaved caspase-3 blot). (**b**) Dotplot showing the moi of every silencing level used. (**c**) *CDT2* levels decreased progressively with the gradual silencing (arrow: *CDT2*-specific band; arrowhead: unspecific band). (**d**) S-phase cell population gradually decreased with the *CDT2* silencing level (left panel, linear regression of both factors) while apoptosis was gradually induced (right panel), especially in TC32 cell line. **t*-test for differences between RM82- and TC32-induced apoptosis, *P*-value < 0.05. (**e**) siRNA knockdown of *CDT2* (left panel: *CDT2* blot, arrow: *CDT2*-specific band; arrowhead: unspecific band) reproduced the effects on cell cycle (central panel) and apoptosis (right panel) of the shRNA lentiviral approach. (**f**) *CDT2* ectopic overexpression in STAET2.1 (left panel, barplot: levels of *CDT2* normalized to β-tubulin levels, blot quantification) resulted in a proliferation increase (central panel: 5-day MTT assay, pBABE-*CDT2* absorbance/pBABE-empty absorbance at every time point) and a decrease in the G2/M cell population (right panel). β-tub, beta-tubulin; ET2.1, STAET2.1 cell line; shRNA, small hairpin RNA; siRNA; small interfering RNA; pB, pBABE. In all cases average of duplicates and measures expressed as mean ± s.d. **t*-test *P*-value <0.05.

observed *in vitro* (Figure 5b), although the differences found between the silencing levels were attenuated due to a higher dispersion of the *in vivo* data (*post hoc* tests found differences between the 100 and 50% silencing levels, *P*-value <0.05). *t*-Test analysis validated the effect on proliferation of the *in vivo CDT2* knockdown. Moreover, the highest silencing level exhibited dramatic effects *in vivo*, achieving an almost complete suppression of tumor growth in several of the animals (Figure 5c).

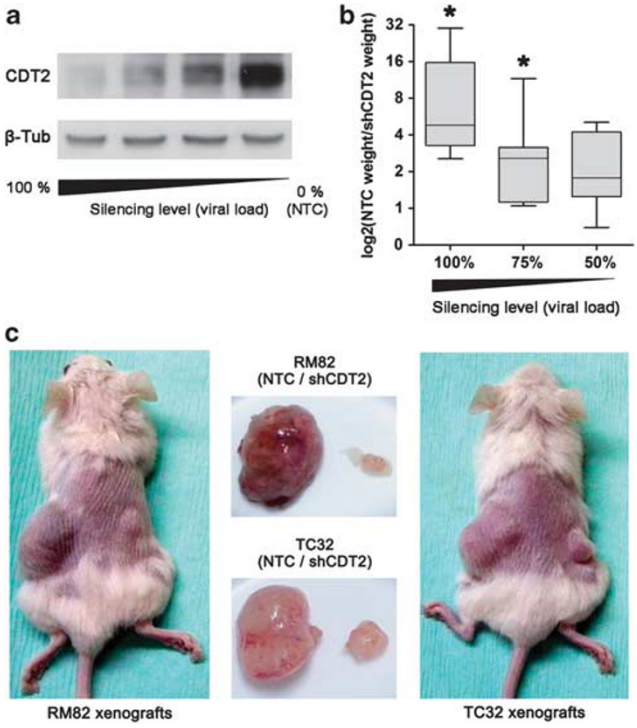

Figure 5 *In vivo CDT2* knockdown confirmed the dependence of 1qG ES cell lines on *CDT2* levels for their proliferation. (**a**) Western-blot validation of *CDT2* progressively decreased according to the silencing level, in RM82 protein extracts. (**b**) Boxplot summarizing the difference in tumor weight (log2(NTC weight/sh*CDT2* weight)) obtained by each *CDT2* silencing level. **t*-test for one sample (H0 = 0), *P*-value <0.05. (**c**) *CDT2* full silencing almost completely suppressed tumor proliferation in several xenografts (NTC tumor on the left flank, shCDT2 tumor on the right flank). Left panel: RM82 xenografts 19 days after injection; central panel: tumors excised from the animals shown in the pictures; right panel: TC32 xenografts 19 days after injection. β-tub, beta-tubulin; NTC, non-targeting control.

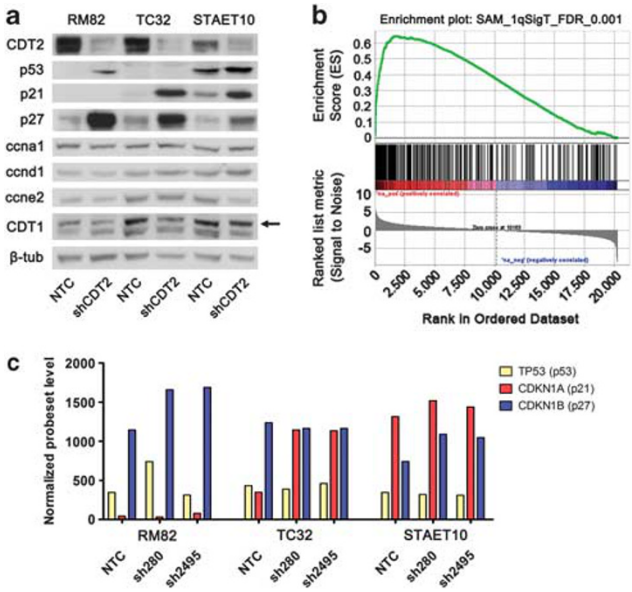

Figure 6 *CDT2* knockdown induced dramatic increases in the protein levels of several G1 to S transition inhibitors, known targets of the CUL4/DDB1^{CDT2} complex, and the expression profile resulting from the *CDT2* knockdown is highly similar to the 1qGSigT differential expression profile. (**a**) Western-blot of several G1 to S transition regulators, demonstrating the specific increases in *p53*, *p21* and *p27* after *CDT2* knockdown (arrow: specific *CDT1* band). (**b**) GSEA enrichment plot demonstrating a significant overlap between the differential expression profiles of *CDT2*-silenced ES cell lines and 1qGSigT. (**c**) *p53*, *p21* and *p27* probeset levels from expression microarrays, unable to explain the changes observed in the protein levels of these cell cycle inhibitors.

CDT2 *knockdown induces dramatic changes in the protein levels of several G1 to S transition inhibitors that are known specific targets of the CUL4/DDB1^{CDT2} complex*

RM82, TC32 and STAET10 (a cell line which also bears the 1qG and high *CDT2* levels; Supplementary Figure S4D) were subjected to a western-blot screening aimed at identifying changes in protein levels (Figure 6a) in response to the *CDT2* knockdown. Antibodies recognizing several G1 to S regulators, including some well-characterized targets of the CUL4/DDB1^{CDT2} complex, were used.

As a result of this assay, only proteins previously described as targets of the CUL4/DDB1^{CDT2} complex (*p21*, *p27* and *p53*) displayed changes in their levels after *CDT2* knockdown, offering a mechanistic explanation and confirming the specificity of the data obtained in the *in vitro* and *in vivo* assays. Moreover, the changes detected with this blot screening were due to post-transcriptional processes, as the levels of *p21*, *p27* and *p53* probesets (from the expression microarray analysis, see below) showed only slight variations in response to the *CDT2* knockdown (maximum a three-fold increase of *p21* in TC32; see Figure 6c), unable to account for the observed changes in protein levels (of hundreds of times). This finding is again consistent with the reported function of the CUL4/DDB1^{CDT2} complex, which exerts a post-traductional modification of its specific targets as a signal for their posterior degradation in the proteasome 26S (Haas and Rose, 1982).

Besides, the response in the different cell lines was heterogeneous, reflecting their diverse molecular backgrounds (Figure 6a, TC32 seems to lack *p53* protein expression while RM82 showed no *p21* at all, both at transcript and protein levels). The double-banded pattern of *CDT2* blot shown in Figures 4a and c (bottom panel), 5a and 6a appears when long electrophoresis times are applied and is probably reflecting the predicted existence of several transcript isoforms arising from a same locus (both bands respond to the *CDT2* knockdown). Conversely, when shorter times are used a *CDT2* single-banded pattern is detected (arrows in Figures 4c, top panel and e) along with an unspecific band close to it (arrowheads in Figures 4c, top panel and e).

A significant overlap between the differential expression profiles of CDT2*-silenced ES cell lines and 1qGSigT suggests a major contribution of* CDT2 *to the molecular phenotype linked to 1qG*

Expression microarray analysis was conducted using RNA from *CDT2*-silenced ES cell lines (RM82, TC32

and STAET10) and their respective controls (NTCs), and a differential expression profile due to the knockdown of *CDT2* was obtained. This profile was compared with the 1qGSigT differential expression profile (Supplementary File 1, Spreadsheet #6), using GSEA as described in Supplementary Material and methods. A significant overlap between both profiles was found as reflected by the high enrichment score obtained (normalized enrichment score = 3.16, FDR q-value <0.001). Indeed, *CDT2* knockdown was able to significantly decrease the expression level of 40% of the 1qGSigT differential profile (Supplementary File 1, Spreadsheet #7). This result revealed a strong contribution of *CDT2* to the expression profile associated with 1qG, pointing to its condition as a major responsible for the molecular phenotype linked to this CNA. GSEA enrichment plot is shown in Figure 6b.

Discussion

Here we report a collaborative study of a large number of ES samples aimed at identifying subsets of patients with poor prognosis based on their molecular features. This study demonstrates the dramatic impact of the CNAs on ES clinical outcome and identifies 1qG as the most clinically relevant CNA. Transcriptomic reanalyses enabled the validation of this finding in an independent set of ES tumors and led us to unveil a cell cycle deregulation expression pattern linked to the 1qG. *In vitro* and *in vivo* validations of a candidate gene, *CDT2* (the main overexpressed gene in 1qGT), not only confirmed empirically the bioinformatics findings, but also pointed to a major role of this gene in the molecular and clinical phenotype distinctive of this ES subtype.

Regarding the biological meaning of the findings here reported, cell cycle regulation is the main target of both EWS-ETS (Kauer *et al*., 2009) and previously known ES secondary alterations (*CDKN2A* deletions and *TP53* mutations). Moreover, 1qG/*CDT2* overexpression also hit this same cellular function. Taken together, these evidences suggest that ES secondary genetic alterations cooperate with EWS-ETS to overcome cell cycle progression inhibitors. In line with this idea, we propose a molecular model (Supplementary Figure S6) to explain how 1qG, especially through *CDT2* overexpression, could contribute to the worse clinical outcome of the ES with 1qG. According to this model, 1qG/*CDT2* overexpression could confer a growth advantage by means of *CDT2* potent effects depleting the levels of multiple cell cycle inhibitors. However, this is a preliminary model, which requires further experimental insights to precisely define the molecular contribution of 1qG and protein ubiquitination functions to the ES biology. Additional interpretation of 1qG/*CDT2* results is discussed in the Supplementary Information file.

On the other hand, we expect that the conclusions from the present work will eventually lead to benefits for this substantial subset of ES patients in two ways. First, the potential of the 1qG CNA and/or *CDT2* overexpression as a negative prognostic biomarker; conversely, the absence of CNAs could be used as a reliable marker of good prognosis. Second, the suitability of $CUL4/DDB^{CDT2}$ complex for targeted therapy, as a new promising therapeutic compound that inhibits cullin-ring ligases activity has been developed (Soucy *et al*., 2009).

Besides, our findings could also contribute to understand the biology of other neoplasms in which 1qG has been related to an adverse clinical outcome (Hing *et al*., 2001; Kjellman *et al*., 2001; Lo *et al*., 2007; Pezzolo *et al*., 2009; Balcarkova *et al*., 2009), as the mechanisms involved could be similar to those described here.

We have thus reported that 1qG defines a subset of ES patients with an adverse clinical outcome, and shown that subsequent overexpression of *CDT2*, a gene involved in cell cycle control, is a major actor in the cell cycle deregulation and increased proliferation rates that constitute the hallmarks of this ES subtype. Both molecular findings are potentially useful as prognostic biomarkers.

Materials and methods

Patients and samples

Tumor set 1 comprised 66 ES primary tumors and 1 pulmonary metastasis collected at two institutions of the EuroBoNet consortium (Catholic University of Leuven, $n=40$; Heinrich-Heine-University, $n=27$). Forty-four patients were males and 23 females, with ages from 1 to 84 years (median age = 15), with primary tumors localized in bones ($n=47$) and soft tissues ($n=19$). Seventeen patients were diagnosed for primary disseminated disease. The diagnosis was performed by experienced sarcoma pathologists and all tumor specimens were confirmed to bear the EWS-ETS by fluorescence *in situ* hybridization, using split-apart EWS probe (Abbott Laboratories, Chicago, IL, USA), or by RT–PCR (Friedrichs *et al*., 2006). Correlation of classical clinical parameters (primary tumor location, presence of metastasis, and others) with survival was assessed to ensure they were the usual ones for this tumor entity. Please refer to Supplementary Material and methods for a description of patient treatment.

Approval of the Ethics Committees involved is available in all cases and written informed consent was obtained before registration of the patients. A description of tumor set 2 ($n=38$), used in the transcriptomic studies and in the tissue microarray elaboration, can be found elsewhere (Scotlandi *et al*., 2009).

Cell lines

ES cell lines used were A4573, A673, CADO-ES, CHP-100, EW3, RDES, RM82, SKES1, SKNMC, STAET1, STAET2.1, STAET10, TC71, TTC466, TC32, VH64 and WE68, which were obtained from the EuroBoNet cell line panel that is maintained and regularly checked and characterized by Ottaviano *et al*. in Heinrich-Heine-University at Düsseldorf, by the methods explained in reference (Ottaviano *et al*., 2010).

Array comparative genomic hybridization

Whole-genome aCGH studies were performed using the Sanger 1 Mb clone set. BAC DNA was extracted, amplified by degenerate oligonucleotide primed (DOP) and aminolinking-PCR, and triplicate aliquots were spotted onto Codelink slides (Amersham, GE, Piscataway, NJ, USA).

Tumor and reference DNA (an equimolar DNA pool from 100 healthy donors, obtained from the Spanish National DNA Bank after approval by its External Ethics Committee) was Cy5/Cy3-dCTP-labelled (Amersham, GE) using a non-commercial Random Priming kit composed of random octamers dissolved in Exo-Minus Klenow buffer (Epicentre, Madison, WI, USA), a dNTPs mix depleted in dCTP (Eppendorf, Hamburg, Germany) and Exo-Minus Klenow enzyme (Epicentre). Labelled DNA was purified through Illustra G-50 Microspin Columns (Amersham, GE), mixed and then precipitated along with Cot-1 Human DNA (Roche Applied Sciences, Penzberg, Germany). Hybridization was performed for 48 h at 42 °C and the excess probe was removed.

A full description of the aCGH analysis procedures is included in Supplementary Material and Methods.

The microarray data (from BAC microarrays, SNP microarrays and expression microarrays) generated in this study has been deposited in the NCBI's Gene Expression Omnibus (GEO; http://www.ncbi.nlm.nih.gov/geo/) and is accessible through GEO Series accession number GSE20368.

Tumor set 2 genomic dataset, belonging to a subset of 14 tumors with previously generated CNA profiles (Savola *et al*., 2009), was obtained from the public CanGEM repository (http://www.cangem.org) with the entry code CG-SER-18.

Conflict of interest

The authors declare no conflict of interest.

Acknowledgements

Centro de Investigación del Cáncer-IBMCC, Heinrich-Heine-University Duesseldorf, Catholic University of Leuven, University of Valencia, Istituti Ortopedici Rizzoli, University of Helsinki, Leiden University Medical Center and University Children's Hospital Muenster are partners of the EuroBoNeT consortium, a network of excellence granted by the European Commission for studying the pathology and genetics of bone tumors. Daniel J Garcia-Domínguez is supported by a grant from the Maria Garcia-Estrada Foundation. Research in Enrique de Alava's lab is also supported by the Ministry of Science and Innovation of Spain-FEDER (PI081828, RD06/0020/0059). Trial center Muenster is supported by grants from Deutsche Krebshilfe, 50-2551 Jü3 und 50-2551-Jü4 and Federal Ministry of Education and Research Germany, BMBF (TranSaRNet) 01GM0869, Deutsches Zentrum für Luft- und Raumfahrt e.V. We thank Dr Hung-Wei Pan and Dr Hey-Chi Hsu (Department of Pathology, College of Medicine, National Taiwan University, Taipei, Taiwan) for the anti-*CDT2* antibody and pBABE-*CDT2* construction. Thanks are due to Cristina Teodosio and Martín Perez de Andrés for their kind help with the flow cytometer, to Andreas Ranft for helping with the clinical data, to Agustín Mayo Iscar for his help with statistics, and to Antonella Chiechi, Alicia Ginel and Alberto de Luis for their advice.

Author contributions: C Mackintosh made the experimental design, carried out most of the experiments, analyzed the data, wrote the R code, obtained the conclusions and wrote the manuscript; JL Ordóñez and DJ García manipulated the animals; V Sevillano replicated and amplified the shRNA construction collection and other retro and lentiviral vectors; A Llombart-Bosch performed and evaluated the Ki-67 IHC; K Szuhai carried out the COBRA-FISH analysis. M Debiec-Rychter, KL Schaefer, K Scotlandi, P Picci, U Dirksen, R Sciot, M Alberghini, F Sinnaeve, S Knuutila and PCW Hogendoorn supplied tumor samples, cell lines, clinical information, raw data from microarrays and revised the manuscript. E de Alava supervised the studies, coordinated the joint effort and revised the manuscript.

References

Abbas T, Sivaprasad U, Terai K, Amador V, Pagano M, Dutta A. (2008). PCNA-dependent regulation of p21 ubiquitylation and degradation via the CRL4Cdt2 ubiquitin ligase complex. *Genes Dev* **22**: 2496–2506.

Aurias A, Rimbaut C, Buffe D, Zucker JM, Mazabraud A. (1984). Translocation involving chromosome 22 in Ewing's sarcoma. A cytogenetic study of four fresh tumors. *Cancer Genet Cytogenet* **12**: 21–25.

Balcarkova J, Urbankova H, Scudla V, Holzerova M, Bacovsky J, Indrak K *et al*. (2009). Gain of chromosome arm 1q in patients in relapse and progression of multiple myeloma. *Cancer Genet Cytogenet* **192**: 68–72.

Banks D, Wu M, Higa LA, Gavrilova N, Quan J, Ye T *et al*. (2006). L2DTL/CDT2 and PCNA interact with p53 and regulate p53 polyubiquitination and protein stability through MDM2 and CUL4A/DDB1 complexes. *Cell Cycle* **5**: 1719–1729.

Brisset S, Schleiermacher G, Peter M, Mairal A, Oberlin O, Delattre O *et al*. (2001). CGH analysis of secondary genetic changes in Ewing tumors: correlation with metastatic disease in a series of 43 cases. *Cancer Genet Cytogenet* **130**: 57–61.

Delattre O, Zucman J, Plougastel B, Desmaze C, Melot T, Peter M *et al*. (1992). Gene fusion with an ETS DNA-binding domain caused by chromosome translocation in human tumours. *Nature* **359**: 162–165.

Ferreira BI, Alonso J, Carrillo J, Acquadro F, Largo C, Suela J *et al*. (2008). Array CGH and gene-expression profiling reveals distinct genomic instability patterns associated with DNA repair and cell-cycle checkpoint pathways in Ewing's sarcoma. *Oncogene* **27**: 2084–2090.

Friedrichs N, Kriegl L, Poremba C, Schaefer KL, Gabbert HE, Shimomura A *et al*. (2006). Pitfalls in the detection of t(11;22) translocation by fluorescence *in situ* hybridization and RT-PCR: a single-blinded study. *Diagn Mol Pathol* **15**: 83–89.

Haas AL, Rose IA. (1982). The mechanism of ubiquitin activating enzyme. A kinetic and equilibrium analysis. *J Biol Chem* **257**: 10329–10337.

Haeusler J, Ranft A, Boelling T, Gosheger G, Braun-Munzinger G, Vieth V *et al*. (2010). The value of local treatment in patients with primary, disseminated, multifocal Ewing sarcoma (PDMES). *Cancer* **116**: 443–450.

Hattinger CM, Rumpler S, Ambros IM, Strehl S, Lion T, Zoubek A *et al*. (1996). Demonstration of the translocation der(16)t(1;16)(q12;q11.2) in interphase nuclei of Ewing tumors. *Genes Chromosomes Cancer* **17**: 141–150.

Hattinger CM, Potschger U, Tarkkanen M, Squire J, Zielenska M, Kiuru-Kuhlefelt S *et al*. (2002). Prognostic impact of chromosomal aberrations in Ewing tumours. *Br J Cancer* **86**: 1763–1769.

Higa LA, Banks D, Wu M, Kobayashi R, Sun H, Zhang H. (2006a). L2DTL/CDT2 interacts with the CUL4/DDB1 complex and PCNA and regulates CDT1 proteolysis in response to DNA damage. *Cell Cycle* **5**: 1675–1680.

Higa LA, Wu M, Ye T, Kobayashi R, Sun H, Zhang H. (2006b). CUL4-DDB1 ubiquitin ligase interacts with multiple WD40-repeat proteins and regulates histone methylation. *Nat Cell Biol* **8**: 1277–1283.

Higa LA, Yang X, Zheng J, Banks D, Wu M, Ghosh P *et al*. (2006c). Involvement of CUL4 ubiquitin E3 ligases in regulating CDK inhibitors Dacapo/p27Kip1 and cyclin E degradation. *Cell Cycle* **5**: 71–77.

Hing S, Lu YJ, Summersgill B, King-Underwood L, Nicholson J, Grundy P *et al*. (2001). Gain of 1q is associated with adverse outcome in favorable histology Wilms' tumors. *Am J Pathol* **158**: 393–398.

Huang HY, Illei PB, Zhao Z, Mazumdar M, Huvos AG, Healey JH *et al*. (2005). Ewing sarcomas with p53 mutation or p16/p14ARF homozygous deletion: a highly lethal subset associated with poor chemoresponse. *J Clin Oncol* **23**: 548–558.

Jin J, Arias EE, Chen J, Harper JW, Walter JC. (2006). A family of diverse Cul4-Ddb1-interacting proteins includes Cdt2, which is required for S phase destruction of the replication factor Cdt1. *Mol Cell* **23**: 709–721.

Kauer M, Ban J, Kofler R, Walker B, Davis S, Meltzer P *et al*. (2009). A molecular function map of Ewing's sarcoma. *PLoS ONE* **4**: e5415.

Kim Y, Starostina NG, Kipreos ET. (2008). The CRL4Cdt2 ubiquitin ligase targets the degradation of p21Cip1 to control replication licensing. *Genes Dev* **22**: 2507–2519.

Kjellman P, Lagercrantz S, Hoog A, Wallin G, Larsson C, Zedenius J. (2001). Gain of 1q and loss of 9q21.3-q32 are associated with a less favorable prognosis in papillary thyroid carcinoma. *Genes Chromosomes Cancer* **32**: 43–49.

Knuutila S, Armengol G, Bjorkqvist AM, el-Rifai W, Larramendy ML, Monni O *et al*. (1998). Comparative genomic hybridization study on pooled DNAs from tumors of one clinical-pathological entity. *Cancer Genet Cytogenet* **100**: 25–30.

Kullendorff CM, Mertens F, Donner M, Wiebe T, Akerman M, Mandahl N. (1999). Cytogenetic aberrations in Ewing sarcoma: are secondary changes associated with clinical outcome? *Med Pediatr Oncol* **32**: 79–83.

Le Deley MC, Delattre O, Schaefer KL, Burchill SA, Koehler G, Hogendoorn PC *et al*. (2010). Impact of EWS-ETS fusion type on disease progression in Ewing's sarcoma/peripheral primitive neuroectodermal tumor: prospective results from the cooperative Euro-E.W.I.N.G. 99. *Trial J Clin Oncol* **28**: 1982–1988.

Liu CL, Yu IS, Pan HW, Lin SW, Hsu HC. (2007). L2dtl is essential for cell survival and nuclear division in early mouse embryonic development. *J Biol Chem* **282**: 1109–1118.

Lo KC, Ma C, Bundy BN, Pomeroy SL, Eberhart CG, Cowell JK. (2007). Gain of 1q is a potential univariate negative prognostic marker for survival in medulloblastoma. *Clin Cancer Res* **13**: 7022–7028.

Nishitani H, Shiomi Y, Iida H, Michishita M, Takami T, Tsurimoto T. (2008). CDK inhibitor p21 is degraded by a proliferating cell nuclear antigen-coupled Cul4-DDB1Cdt2 pathway during S phase and after UV irradiation. *J Biol Chem* **283**: 29045–29052.

Ordoñez JL, Osuna D, Herrero D, de Alava E, Madoz-Gurpide J. (2009). Advances in Ewing's sarcoma research: where are we now and what lies ahead? *Cancer Res* **69**: 7140–7150.

Ottaviano L, Schaefer KL, Gajewski M, Huckenbeck W, Baldus S, Rogel U *et al*. (2010). Molecular characterization of commonly used cell lines for bone tumor research: a trans-European EuroBoNet effort. *Genes Chromosomes Cancer* **49**: 40–51.

Ozaki T, Paulussen M, Poremba C, Brinkschmidt C, Rerin J, Ahrens S *et al*. (2001). Genetic imbalances revealed by comparative genomic hybridization in Ewing tumors. *Genes Chromosomes Cancer* **32**: 164–171.

Pezzolo A, Rossi E, Gimelli S, Parodi F, Negri F, Conte M *et al*. (2009). Presence of 1q gain and absence of 7p gain are new predictors of local or metatastic relapse in localized resectable neuroblastoma. *Neuro Oncol* **11**: 192–200.

Ralph E, Boye E, Kearsey SE. (2006). DNA damage induces Cdt1 proteolysis in fission yeast through a pathway dependent on Cdt2 and Ddb1. *EMBO Rep* **7**: 1134–1139.

Roberts P, Burchill SA, Brownhill S, Cullinane CJ, Johnston C, Griffiths MJ *et al*. (2008). Ploidy and karyotype complexity are powerful prognostic indicators in the Ewing's sarcoma family of tumors: a study by the United Kingdom Cancer Cytogenetics and the Children′s Cancer and Leukaemia Group. *Genes Chromosomes Cancer* **47**: 207–220.

Sansam CL, Shepard JL, Lai K, Ianari A, Danielian PS, Amsterdam A *et al*. (2006). DTL/CDT2 is essential for both CDT1 regulation and the early G2/M checkpoint. *Genes Dev* **20**: 3117–3129.

Savola S, Klami A, Tripathi A, Niini T, Serra M, Picci P *et al*. (2009). Combined use of expression and CGH arrays pinpoints novel candidate genes in Ewing sarcoma family of tumors. *BMC Cancer* **9**: 17.

Scotlandi K, Remondini D, Castellani G, Manara MC, Nardi F, Cantiani L *et al*. (2009). Overcoming resistance to conventional drugs in Ewing sarcoma and identification of molecular predictors of outcome. *J Clin Oncol* **27**: 2209–2216.

Soucy TA, Smith PG, Milhollen MA, Berger AJ, Gavin JM, Adhikari S *et al*. (2009). An inhibitor of NEDD8-activating enzyme as a new approach to treat cancer. *Nature* **458**: 732–736.

Subramanian A, Tamayo P, Mootha VK, Mukherjee S, Ebert BL, Gillette MA *et al*. (2005). Gene set enrichment analysis: a knowledge-based approach for interpreting genome-wide expression profiles. *Proc Natl Acad Sci USA* **102**: 15545–15550.

Tarkkanen M, Kiuru-Kuhlefelt S, Blomqvist C, Armengol G, Bohling T, Ekfors T *et al*. (1999). Clinical correlations of genetic changes by comparative genomic hybridization in Ewing sarcoma and related tumors. *Cancer Genet Cytogenet* **114**: 35–41.

Turc-Carel C, Philip I, Berger MP, Philip T, Lenoir GM. (1984). Chromosome study of Ewing's sarcoma (ES) cell lines. Consistency of a reciprocal translocation t(11;22)(q24;q12). *Cancer Genet Cytogenet* **12**: 1–19.

van de Wiel MA, Smeets SJ, Brakenhoff RH, Ylstra B. (2005). CGHMultiArray: exact P-values for multi-array comparative genomic hybridization data. *Bioinformatics* **21**: 3193–3194.

van de Wiel MA, Kim KI, Vosse SJ, van Wieringen WN, Wilting SM, Ylstra B. (2007). CGHcall: calling aberrations for array CGH tumor profiles. *Bioinformatics* **23**: 892–894.

van de Wiel MA, Wieringen WN. (2007). CGHregions: dimension reduction for array CGH data with minimal information loss. *Cancer inform* **3**: 55–63.

van Doorninck JA, Ji L, Schaub B, Shimada H, Wing MR, Krailo MD *et al*. (2010). Current treatment protocols have eliminated the prognostic advantage of type 1 fusions in Ewing sarcoma: a report from the Children′s Oncology Group. *J Clin Oncol* **28**: 1989–1994.

Whang-Peng J, Triche TJ, Knutsen T, Miser J, Douglass EC, Israel MA. (1984). Chromosome translocation in peripheral neuroepithelioma. *N Engl J Med* **311**: 584–585.

Supplementary Information accompanies the paper on the Oncogene website (http://www.nature.com/onc)